

# Computationally Light Spectrally Normalized Memory Neuron Network based Estimator for GPS-Denied operation of Micro UAV

**Nishanth Rao**

Department of Aerospace Engineering  
Indian Institute of Science, Bengaluru India  
nishanthrao@iisc.ac.in

**Suresh Sundaram**

Department of Aerospace Engineering  
Indian Institute of Science, Bengaluru India  
vssuresh@iisc.ac.in

**Varun Raghavendra**

Department of Aerospace Engineering  
Indian Institute of Science, Bengaluru India  
varuncr@iisc.ac.in

**Abstract:** This paper addresses the problem of position estimation in UAVs operating in a cluttered environment where GPS information is unavailable. A model learning-based approach is proposed that takes in the rotor RPMs and past state as input and predicts the one-step-ahead position of the UAV using a novel spectral-normalized memory neural network (SN-MNN). The spectral normalization guarantees stable and reliable prediction performance. The predicted position is transformed to global coordinate frame which is then fused along with the odometry of other peripheral sensors like IMU, barometer, compass etc., using the onboard extended Kalman filter to estimate the states of the UAV. The experimental flight data collected from a motion capture facility using a micro-UAV is used to train the SN-MNN. The PX4-ECL library is used to replay the flight data using the proposed algorithm, and the estimated position is compared with actual ground truth data. The proposed algorithm doesn't require any additional onboard sensors, and is computationally light. The performance of the proposed approach is compared with the current state-of-art GPS-denied algorithms, and it can be seen that the proposed algorithm has the least RMSE for position estimates.

## 1 Introduction

Advancements in UAV technology have enabled their widespread usage in logistic transportation, urban air mobility and agriculture. A crucial aspect of the UAV flight is the accuracy of the onboard navigation system that provides a sense of whereabouts to the UAV controller. The onboard navigation system relies heavily on GPS sensors that accurately estimates the position the UAV. However, in cluttered environments like forests and indoor environments, there is an intermittent loss of GPS (sometimes no GPS signal), which can lead to inaccurate position estimates, rendering the UAV unstable. Thus, it is crucial to look for GPS-denied alternatives to provide reliable position information to the UAV.

The existing literature on algorithms developed for GPS-denied operation can be broadly divided into two categories: algorithms that use reliable position estimates generated by either vision-based systems or simultaneous localization and mapping (SLAM)-based systems. In [1], stereo camera-based localization is employed for fast and agile navigation of the UAV in the presence of surrounding obstacles. In [2] the concept of *image moments* is utilized from environment images to estimate the translational velocity of the UAV reliably. A combination of optical flow and ultrasound sensors has been used in [3] to achieve a stable indoor hovering performance of a micro aerial vehicle. However, vision-based localization systems fail to provide reliable odometry in varying lighting conditions and exhibit drift when no features are available to track. Further, one needs to tune the parameters meticulously to achieve reliable performance in a known environment[4].

On the other hand, SLAM-based methods mostly require LiDAR sensors or compatible vision-based sensors. In [5], a 6-DOF SLAM is proposed that builds a relative map from surrounding features and provides odometry measurements relative to this map. In [6], a vision-based SLAM algorithm is employed using a monocular camera and an ultrasound camera for navigation. To alleviate the problems specific to vision-based sensors, [7] employs an infrared thermal sensor to obtain localization information in the presence of dark, texture-less environments with dust-filled / smoke-filled settings. However, SLAM-based methods work efficiently only in a cluttered environment with some external objects that can be tracked throughout the flight. When flying in areas without any surrounding objects or in fast dynamic environments, vision-based odometry and SLAM-based methods fail to provide accurate position estimates to the UAV. Reliable vision-based odometry systems require high FPS performance cameras that are prohibitively expensive. Moreover, these methods require additional onboard specialized sensors that can be limiting in a micro-UAV setting, and tend to consume extra power that can limit the overall endurance of the UAV.

In this paper, a *data-driven model learning*-based approach is proposed to estimate the UAV position using a Spectrally Normalized Memory Neuron Network (SN-MNN) that is invariant to the environmental features and external factors like surrounding objects, varying lighting conditions etc. The SN-MNN predicts the position of the UAV based on the rotor RPM input and previous UAV states. It is shown theoretically that spectral normalization guarantees a stable prediction performance by constraining the Lipschitz constant of the fitted function. The look-ahead predicted position is transformed to a global coordinate, and extended Kalman filter-based state fusion is used to estimate the UAV states. The experimental flight data from a motion capture facility is used for training the SN-MNN. The model learning-based approach is validated using Pixhawk replay on the experimental flight data. Finally, the performance of the proposed algorithm is compared with other state-of-art GPS-denied algorithms, and possible limitations and future directions are discussed.

## 2 Spectral-Normalized Memory Neuron Network based State Estimation

First, this section presents the UAV dynamic equations and input-output model. Next, the novel data-driven spectrally normalized memory neuron network is presented to predict the position of the UAV from the past state and current input. Finally, the predicted local position is converted to global coordinates (GPS) and state fusion is carried out to estimate the UAV states.

### 2.1 Input-Output Model of UAV

The physics-based mathematical model of a typical UAV system is given below:

$$\begin{aligned} \dot{\mathbf{x}} &= \mathbf{v}, \quad m\dot{\mathbf{v}} = mg\hat{\mathbf{k}} + \mathbf{R}\hat{\mathbf{k}}f_t + \tilde{\mathbf{f}} & (1a) \\ \dot{\mathbf{R}} &= \mathbf{R}\boldsymbol{\Omega}^\times, \quad \mathbf{J}\dot{\boldsymbol{\Omega}} + \boldsymbol{\Omega}^\times\mathbf{J}\boldsymbol{\Omega} = \boldsymbol{\tau} + \tilde{\boldsymbol{\tau}} & (1b) \\ \text{with, } f_t &= K_\omega (\omega_1^2 + \omega_2^2 + \omega_3^2 + \omega_4^2) & (1c) \\ \boldsymbol{\tau} &= \begin{bmatrix} \tau_x \\ \tau_y \\ \tau_z \end{bmatrix} = \begin{bmatrix} K_\omega l (\omega_3^2 - \omega_1^2) \\ K_\omega l (\omega_4^2 - \omega_2^2) \\ K_d (\omega_2^2 + \omega_4^2 - \omega_1^2 - \omega_3^2) \end{bmatrix} & (1d) \end{aligned}$$

where  $\hat{\mathbf{k}} = [0 \ 0 \ 1]^T$  is the unit vector along the  $z$ -axis,  $\mathbf{x} \in \mathbb{R}^3$  is the position of the UAV with mass  $m \in \mathbb{R}$  and moment of inertia  $\mathbf{J} \in \mathbb{R}^{3 \times 3}$ ,  $\mathbf{v} \in \mathbb{R}^3$  is the linear velocity,  $\mathbf{R} \in \mathbb{R}^{3 \times 3}$  is the rotation matrix that converts a vector from the UAV-fixed body frame to the inertial frame,  $\boldsymbol{\Omega} \in \mathbb{R}^3$  is the angular velocity of the UAV,  $f_t \in \mathbb{R}$  is the input thrust vector and  $\boldsymbol{\tau} \in \mathbb{R}^3$  is the input torque vector given by Eq. (1c) and (1d) respectively. The quantities  $\omega_i$  denotes the rotational velocity of the  $i^{th}$  motor in (rad/s),  $l$  denotes the arm length of the UAV, and the constants  $K_\omega, K_d$  denote the motor constant and the drag coefficient respectively. The operator  $(\cdot)^\times : \mathbb{R}^3 \rightarrow \mathbb{R}^{3 \times 3}$  is the hat operator that converts a vector to a skew-symmetric matrix. The quantities  $\tilde{\mathbf{f}}, \tilde{\boldsymbol{\tau}}$  represent the external complex aerodynamic forces and torques on the UAV that are mostly unknown or cannot be analytically modelled. In real world, the dynamics given by Eq. (1) are rudimentary and cannot be relied upon for estimating the UAV states due to presence of noise, model uncertainties and external disturbances.

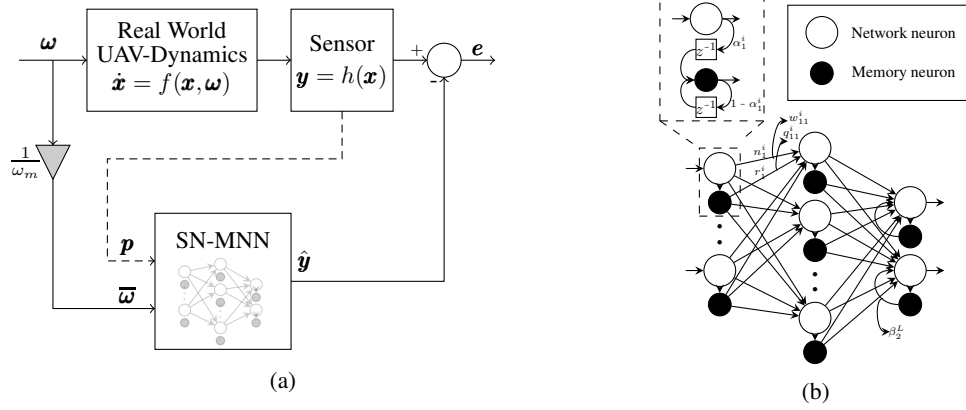


Figure 1: Figure on the left shows a schematic block diagram of SN-MNN training. The error is used for backpropagation. The motor input  $\omega$  is normalized by the maximum rotor speed  $\omega_m$  before feeding to the SN-MNN. Figure on the right shows the schematic diagram of a fully connected SN-MNN consisting of a single hidden layer.

In general, one can use *billings theorem* [8] to write the input-output model of a dynamical system as:

$$\mathbf{y}_{k+1} = f(\mathbf{y}_k, \dots, \mathbf{y}_{k-n}, \mathbf{u}_k, \dots, \mathbf{u}_{k-n}) \quad (2)$$

where  $f(\cdot)$  is an unknown nonlinear function,  $n$  is the order of the system,  $\mathbf{y}_k$  and  $\mathbf{u}_k$  is the output of and input to the system respectively at time step  $k$ . Note that one can use a recurrent neural network to approximate the unknown nonlinear function using the current input and past output. It has been shown in the literature that the *Memory Neuron Network* (MNN) [9] is more efficient in approximating the dynamics accurately than other state-of-the-art recurrent neural networks [10]. The presence of uncertainty in thrust and the unknown disturbance influences the stability/reliability of prediction. The next section proposes a spectrally normalized MNN to learn the UAV model accurately.

## 2.2 Spectral-Normalized Memory Neural Network based Model Learning

The Spectrally Normalized Memory Neural Network (SN-MNN) contains *fully connected* network neurons (white circle) with its associated memory neurons (black solid circle). The unique nature of connection between the Network Neurons and the Memory Neurons (see Fig. 1b) makes the network *recurrent* in nature. The network is parameterized by  $\theta = \{(^1W, ^1Q), \dots, (^LW, ^LQ)\}$ , the weights corresponding to both the network neurons ( $W$ ) as well as the memory neurons ( $Q$ ). The left superscript denotes the layer number. Thus, the output of SN-MNN to an input  $p$  can be compactly represented as:

$$f(p, \theta) = {}^L W (\dots \phi({}^2 W (\phi({}^1 W p + {}^1 Q^1 r)) + {}^2 Q^2 r) \dots) + {}^L Q^L r \quad (3)$$

where  $\phi(\cdot)$  denotes the activation function and  ${}^l r$  denotes the output of the memory neurons present in the  ${}^{lth}$  layer. The recurrence relationship between the memory neurons and the network neurons can be represented as:

$${}^l r_k = {}^l \alpha {}^l n_{k-1} + (1 - {}^l \alpha) {}^l r_{k-1} \quad (4)$$

where  ${}^l n = \phi(\cdot)$  is the output of the activation function in the  ${}^{lth}$  layer and  ${}^l \alpha$  is the weight of the feedback connections between the network and the memory neurons in the  ${}^{lth}$  layer (see Fig. 1b).

The Lipschitz constant  $\gamma$  of a real valued function  $f : \mathbb{R}^n \rightarrow \mathbb{R}$  is defined mathematically as:

$$\|f(p_2) - f(p_1)\|_2 \leq \gamma \|p_2 - p_1\|_2 \quad (5)$$

The Lipschitz constant of a differentiable function is the *maximum spectral norm* of its Jacobian over the function's domain:  $\gamma = \sup_p \rho(\nabla f(p))$ , where  $\rho(A)$  denotes the spectral norm of the matrix  $A$  which is defined as the square root of maximum eigenvalue of the matrix  $A^H A$ . As demonstrated

in [11], it is essential to limit the Lipschitz constant of a neural network to ensure stable reliable prediction performance that is comparable with the actual dynamics of the UAV. The following Theorem guarantees the Lipschitz constant of the SN-MNN:

**Theorem 1.** *The Lipschitz constant of the entire spectrally normalized memory neuron network satisfies the inequality  $\|f(\mathbf{p}, \boldsymbol{\theta})\|_2 \leq \gamma$  under the spectral weight normalization:*

$$\overline{\mathbf{W}} = \left( \frac{\mathbf{W}}{\rho(\mathbf{W})} \right) \cdot \gamma^{\frac{1}{L}}, \quad \overline{\mathbf{Q}} = \left( \frac{\mathbf{Q}}{\rho(\mathbf{Q})} \right) \cdot \gamma^{\frac{1}{L}} \quad (6)$$

with  $\gamma$  being the intended Lipschitz constant of the network, and  $\tanh(\cdot)$  as the activation function.

*Proof.* The spectral norm of a linear map  $g(\mathbf{p}) = \mathbf{W}\mathbf{p} + \mathbf{b}$  can be simplified as:  $\sup_{\mathbf{p}} \rho(\nabla g) = \sup_{\mathbf{p}} \rho(\mathbf{W}) = \rho(\mathbf{W})$ . Moreover, using the inequality  $\text{Lip}(g_1 \circ g_2) \leq \text{Lip}(g_1) \cdot \text{Lip}(g_2)$  and the fact that  $\text{Lip}(\tanh(\cdot)) = 1$  along with Eq. (3) leads to:

$$\|f(\mathbf{p}, \boldsymbol{\theta})\|_2 = \text{Lip} \left( {}^L\overline{\mathbf{W}} \cdot \left( \dots \phi \left( {}^2\overline{\mathbf{W}} \cdot \left( \phi \left( {}^1\overline{\mathbf{W}}\mathbf{p} + {}^1\overline{\mathbf{Q}}\mathbf{r} \right) \right) + {}^2\overline{\mathbf{Q}}\mathbf{r} \right) \dots \right) + {}^L\overline{\mathbf{Q}}\mathbf{r} \right) \quad (7)$$

$$\leq \prod_{l=1}^L \rho(\overline{\mathbf{W}}) = \prod_{l=1}^L \gamma^{\frac{1}{L}} = \gamma \quad (8)$$

Here, the term  ${}^i\overline{\mathbf{Q}}\mathbf{r}$  can be considered as a "time-varying" bias that is independent of input  $\mathbf{p}_k$  at current time step  $k$ , and thus, doesn't affect the Lipschitz constant. However, the term  $\mathbf{r}$  depends on  $\mathbf{p}_{k-1}$  through Eq. 4 which is why the weight matrix  $\mathbf{Q}$  corresponding to the memory neurons must also undergo spectral normalization.  $\square$

For training the network, the *modified backpropagation* approach as described in [9] is used, with the following cost function being minimized during training at every time step:

$$\boldsymbol{\theta}^* = \underset{\boldsymbol{\theta}}{\text{argmin}} \sum_{k=1}^N \frac{1}{T} \|\mathbf{y}_k - f(\mathbf{p}_k, \boldsymbol{\theta})\|_2^2 \quad (9a)$$

$$\text{such that, } \|f(\mathbf{p}_k, \boldsymbol{\theta})\|_2 \leq \gamma \quad (9b)$$

where the input  $\mathbf{p}_k = [\mathbf{y}_{k-1}^T \ \overline{\boldsymbol{\omega}}_k^T \ \boldsymbol{\Theta}_k^T]^T$  consists of the previous position of the UAV  $\mathbf{y}_{k-1} \in \mathbb{R}^3$ , the roll-pitch-yaw orientation of the UAV  $\boldsymbol{\Theta}_k \in \mathbb{R}^3$  and the current normalized motor RPM  $\overline{\boldsymbol{\omega}}_k \in \mathbb{R}^4$ . The training process of the network is illustrated in Fig. 1a. Let  $\mathbf{e}$  be the error vector. Due to the constraint of Eq. (9b), the update rules for  $\mathbf{W}$  and  $\mathbf{Q}$  are as follows:

$${}^l\mathbf{W}_{k+1} = \frac{\gamma^{\frac{1}{L}}}{\rho({}^l\mathbf{W}_k)} ({}^l\mathbf{W}_k - \eta \cdot {}^l\mathbf{n}_k \mathbf{e}^T) \quad (10)$$

$${}^l\mathbf{Q}_{k+1} = \frac{\gamma^{\frac{1}{L}}}{\rho({}^l\mathbf{Q}_k)} ({}^l\mathbf{Q}_k - \eta \cdot {}^l\mathbf{r}_k \mathbf{e}^T) \quad (11)$$

More details of the update rule derivation are provided in the supplementary material.

### 2.3 GPS Conversion and State Estimation

The network predicts the position of the UAV based on the rotor RPM input. This position estimate can be used during *state fusion* typically performed by an onboard Extended Kalman Filter (EKF), in addition to the state information provided by other peripheral sensors like IMU, compass, magnetometer, airflow sensor etc. In this work, the position estimates given by the network are converted to *GPS coordinates*  $\boldsymbol{\zeta}_k$ , also known as geodetic coordinates (latitude, longitude, altitude) and transformed GPS coordinates are used by the EKF for state estimation. This is illustrated in Fig. 2a and Fig. 3. Since many flight controllers offer out-of-box support for real-time GPS fusion, it has been adopted in this paper. Moreover, ground control software utilises GPS coordinates to visualise the UAV path and monitor its itinerary and the course of navigation.

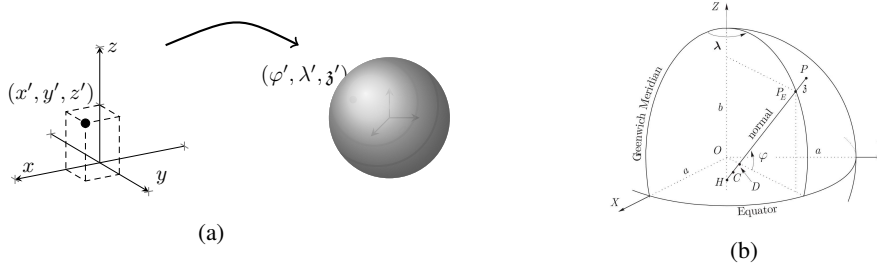


Figure 2: Figure on the left shows the GPS Conversion from East-North-Up (ENU) coordinate vector  $\mathbf{x} = (x', y', z')$  shown in to geodetic (latitude, longitude and altitude) coordinate vector  $\boldsymbol{\zeta} = (\varphi', \lambda', \mathfrak{z}')$ . Figure on the right shows the ECEF coordinate system and the geodetic coordinate system together.

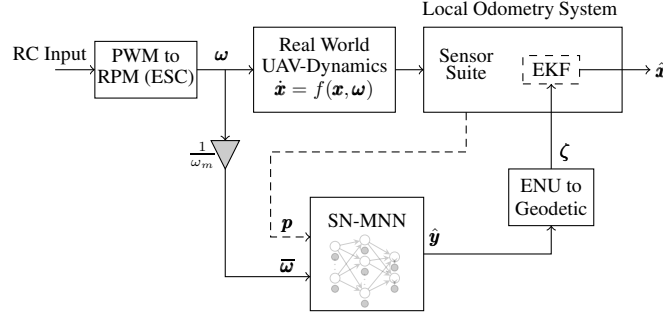


Figure 3: Figure illustrates the state fusion replay process. Based on the RPM input, orientation of the UAV and the previous position of the UAV, the trained SN-MNN predicts the position of the UAV, which is provided to the onboard EKF as GPS coordinates. The Sensor suite consists of peripheral sensors like IMU, compass, magnetometer etc., and the state fusion process is performed by the EKF.

The local position  $\mathbf{y}_k = [x_k \ y_k \ z_k]^T$  predicted by the SN-MNN is in the *East-North-Up* (ENU) coordinate system, as shown in the Fig. 2a. In order to convert them into geodetic coordinate vector  $\boldsymbol{\zeta}_k$ , they must first be converted to the *Earth-Center Earth-Fixed* (ECEF) or *geocentric* coordinate vector  $\mathbf{Y}_k = [X_k \ Y_k \ Z_k]$ . To convert the ENU coordinate vector  $\mathbf{y}_k$  to ECEF coordinate vector  $\mathbf{Y}_k$ , the ECEF coordinate offset vector  $\mathbf{H}^T \mathbf{y}_k$  must be obtained:

$$\mathbf{Y}_k = \mathbf{H}^T \mathbf{y}_k + \mathbf{Y}_0, \text{ where } \mathbf{H} = \begin{bmatrix} -\sin(\lambda_0) & \cos(\lambda_0) & 0 \\ -\cos(\lambda_0)\sin(\varphi_0) & -\sin(\lambda_0)\sin(\varphi_0) & \cos(\varphi_0) \\ \cos(\lambda_0)\cos(\varphi_0) & \sin(\lambda_0)\cos(\varphi_0) & \sin(\varphi_0) \end{bmatrix} \quad (12)$$

where the vector  $\mathbf{Y}_0$  is the initial ECEF coordinate vector. It is assumed that the initial latitude  $\varphi_0$ , the initial longitude  $\lambda_0$  and the initial altitude  $\mathfrak{z}_0$  where the UAV spawns, is known. Thus,  $\boldsymbol{\zeta}_0 = [\varphi_0 \ \lambda_0 \ \mathfrak{z}_0]^T$ . A detailed description of the ECEF coordinate system along with the geodetic coordinate system is given in the supplementary material.

In this paper, the WGS84 *oblate spheroid* model is chosen to approximate the geometry of the earth, with the equatorial radius  $a = 6,378,137m$  and the ellipsoid flattening  $f = 1/298.257223563$ . The WGS84 model is chosen because it is used by the *Global Positioning System* (GPS). The conversion of ECEF coordinates  $\mathbf{Y}_k$  to geodetic coordinate system  $\boldsymbol{\zeta}_k = [\lambda_k \ \varphi_k \ \mathfrak{z}_k]^T$  is a hard problem, which is generally calculated using recursive techniques, but a direct conversion algorithm as proposed in Vermeille [12] is used here as described by the following equations:

$$\boxed{\varphi = 2\tan^{-1}\left(\frac{Z}{D + \sqrt{D^2 + Z^2}}\right); \lambda = 2\tan^{-1}\left(\frac{Y}{X + \sqrt{X^2 + Y^2}}\right); \mathfrak{z} = \frac{\kappa + e^2 - 1}{\kappa}(\sqrt{D^2 + Z^2})} \quad (13)$$

where the parameters  $\kappa$  and  $D$  can be calculated by the set of equations given in the supplementary material. Once the ECEF coordinate vector  $\mathbf{Y}_k$  is calculated, the geodetic coordinate vector  $\boldsymbol{\zeta}_k$  can



Figure 4: Figure on the left shows a snapshot of the MOCAP facility, and figure on the right shows a snapshot of the UAV flight while collecting data.

be obtained using Eq. 13, which is later provided to the local odometry system’s EKF that fuses the information provided by other peripheral sensors like IMU, Compass, Barometer etc., with the predicted geodetic vector  $\zeta_k$  to estimate the states of the UAV. This process is illustrated in Fig. 3.

### 3 Experimental Results

First, this section presents the motion capture setup and the micro-UAV hardware configuration. Next, the experimental flight data collection for training the SN-MNN is discussed. Finally, the performance of SN-MNN prediction, flight evaluation and comparative study results are presented.

#### 3.1 MoCap setup and UAV hardware

The experimental setup consists of a motion capture facility (Phasespace MoCap system) with 24 cameras and a custom-built micro-UAV (generic 250 racer frame) with the Pixhawk 4 Flight Controller that runs on PX4 firmware. The motion capture facility and a micro-UAV operating in the facility are shown in Fig. 4. The micro-UAV is fitted with eight active LED markers for accurate position and orientation estimation with a precision of 0.1mm at 800Hz. The drone weighs about 650 grams, with a RaspberryPi 4 onboard computer. The onboard sensors include an accelerometer, gyroscope, barometer and a compass, all present inside the flight controller. In addition to this, the Velox V2 1950KV T-motors are used with a 5-inch 3 blade propeller configuration.

#### 3.2 Experimental Flight Data Collection and Processing

For training the network, experimental data is collected from the test facility. The states of the UAV and the 4 rotor rpm are logged for multiple flights. The DShot protocol is used by the F55A electronic speed controller (ESC), which measures the rotor RPM values based on the back-EMF from the motor. In total, three hover flights and 4 flights with arbitrary paths are performed manually. Further, five *autonomous flights* are carried out by the onboard raspberry-pi 4 companion computer. These flights ensure that all possible UAV configuration in its state-space are captured.

Next, a common *sampling frequency* is chosen to sample the data corresponding to different sensors (IMU, Barometer, Compass, RPM data and the MOCAP position information). The RPM values are normalized based on the motor’s maximum RPM. The final data consists of 14 columns: one common timestamp for all other columns, 4 normalized rotor rpm (from ESC), position (from MOCAP), orientation and linear velocities (from the IMU and compass) of the UAV. The entire data is then split into training and testing data in the ratio of 2:1. The split of the training and testing data along with the UAV flight trajectory data and their 3D plots are available in the supplementary material.



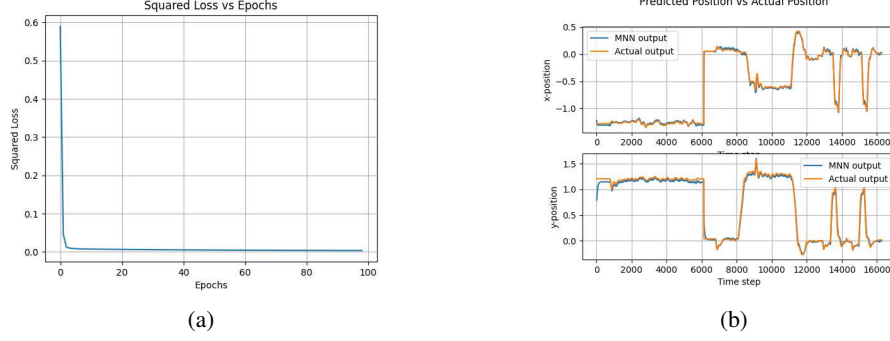


Figure 5: Figure on the left shows the variation of the training loss vs epoch number. Figure on the right shows the prediction of the SN-MNN for the entire testing data set.

### 3.3 SN-MNN Prediction Performance Evaluation

The SN-MNN is trained to predict the one-step-ahead position of the UAV ( $x$ -,  $y$ - coordinates), with the current UAV position  $\mathbf{y}_k \in \mathbb{R}^3$ , orientation (Euler angles)  $\Theta_k \in \mathbb{R}^3$  and the normalized rotor RPM  $\bar{\omega}_k \in \mathbb{R}^4$  as the input to the network. Hence, the selected architecture of SN-MNN is: 10 input neurons, 100 hidden neurons and 2 output neurons. The network neurons in the hidden layer uses  $\tanh(\cdot)$  activation and the network neurons in output layer employ linear activation function. The network is implemented in Python using Numpy Library. The network is trained for a total of 100 epochs. The variation of the squared loss during training is shown in Fig. 5a.

The output of the network for the entire test data (combined into one) is shown in Fig. 5b. The RMSE for the entire prediction is about  $5.84\text{cm}$  with errors in  $x$ - and  $y$ - position being about  $3\text{cm}$  and  $5\text{cm}$  respectively. It can be seen from Fig. 5b that the network has successfully learned the UAV dynamics accurately. The value of the Lipschitz constant  $\gamma$  (here  $\gamma = 1$ ) of the network plays an important role in stabilization of the network during training process. It also determines "how fast" the network output can vary: For eg., if the UAV is mostly hovering and making slow movements, the Lipschitz constant can be set to a low value. If the UAV is performing aggressive sharp maneuvers frequently, then the Lipschitz constant of the network must be set to a high value. In this paper, the trajectory data is collected for a UAV that mostly cruises and exhibits slow maneuvers.

### 3.4 State Fusion and Experimental data evaluation

Once the predicted position  $\mathbf{y}_k$  is obtained from the SN-MNN, the GPS geodetic vector  $\zeta_k$  is calculated from Eq. 13, which is then given to the EKF for state fusion along with other state information like orientation, linear velocities (IMU) and UAV heading (compass). This is illustrated in Fig. 3. The PX4-ECL library [13] provides a "flight replay" MATLAB script that runs the state fusion process from different sensors for the entire flight duration. The raw sensor values from IMU, barometer, GPS and magnetometer are taken during the replay, and the EKF fusion starts. Once completed, the fused estimated states of the UAV are provided for the entire flight duration. It must be noted that during the replay process, the position information from MoCap facility is **not used**, and only the GPS coordinates obtained from the predicted position is used. This EKF implementation is exactly the same as what the PX4 firmware uses, and thus the performance for both the offline replay as well as an actual flight will be very close, as described in [13].

The outputs for the state fusion process using PX4-ECL are shown in Fig. 6 for the Random Flight 3 (R-3). It must be noted that the GPS fusion only affects the position and linear velocity of the UAV, not its rotational components. The estimation plots for other UAV states are provided in the supplementary material. The errors between the estimated positions and the actual positions of the UAV is around  $7.3\text{cm}$ . Further, Table 1 shows a comparison with two state-of-art methods, namely the Visual Inertial Navigation System (VINS) and the Visual Inertial Odometry (VIO). The RMSE reported by these methods are compared along with the proposed method in this work. It can be seen that the RMSE reduces by about 60% for VINS-mono[14] and about 40% for VIO[15]. Further, the algorithm is computationally light, as one has to implement only the trained feedforward SN-MNN model. This implementation can be done directly on the flight controller, requiring no additional

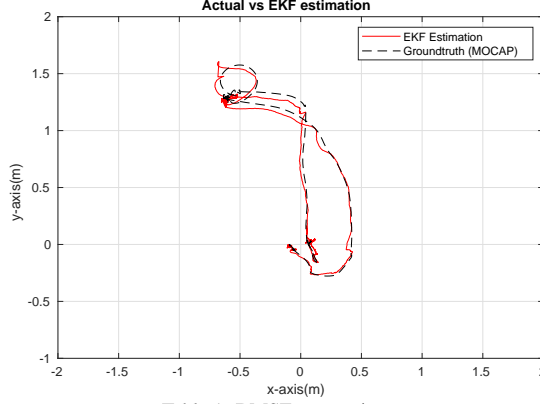


Table 1: RMSE comparison

	VINS-Mono	VIO	SN-MNN + EKF
RMSE (m)	0.18	0.13	<b>0.07</b>

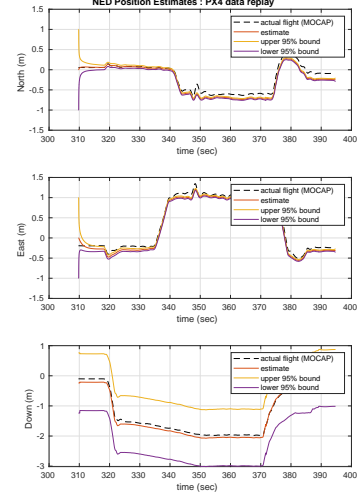


Figure 6: Figure on the left shows the estimated vs actual position of the UAV after EKF replay. Figure on the right shows a detailed plot of positions in individual axis, along with the filter’s estimation bounds ( $\pm 95\%$ ). The table on the left shows the RMSE for two state-of-art GPS-denied methods, namely the VINS fusion and VIO.

onboard computer. Thus, from the above results it can be concluded that the proposed algorithm can be used to estimate the UAV states from the rotor RPM reliably.

**Limitations:** One of the critical requirements for the proposed approach is the generation of training data for the SN-MNN. The reliability of the data and its diversity are important to capture the UAV dynamics accurately. Similar to other GPS-denied algorithms, the absence of wind measurement and other external disturbances influences the prediction performance. Future work will strive to mitigate these issues, making the proposed algorithm more robust. (Please refer the supplementary material for other details and future work with its progress.)

## 4 Conclusion

In this paper, a data-driven model learning-based approach has been proposed to estimate the states of the UAV reliably. The model learning-based algorithm employs a novel spectrally normalized memory neuron network to predict the position of the micro-UAV using rotor RPM and its past state. The predicted position is then transformed into GPS coordinates and fused with other sensor information to estimate the states of the UAV. Experimental flight data from the MoCap facility is used to train the SN-MNN. The performance of the proposed algorithm is compared with state-of-art VIO and VINS-mono algorithms. The results clearly indicate that the proposed algorithm improves the position estimate by reducing the RMSE by approximately 40%. One should also note that the proposed approach is computationally less intensive and does not require any additional onboard sensor; it is independent of environmental features like varying lighting conditions and surrounding obstacles.

## 5 Acknowledgements

## References

- [1] K. Mohta, M. Watterson, Y. Mulgaonkar, S. Liu, C. Qu, A. Makineni, K. Saulnier, K. Sun, A. Zhu, J. Delmerico, et al. Fast, autonomous flight in GPS-denied and cluttered environments. *Journal of Field Robotics*, 35(1):101–120, 2018.
- [2] R. Mebarki and V. Lippiello. Image moments-based velocity estimation of UAVs in GPS denied environments. In *2014 IEEE International Symposium on Safety, Security, and Rescue Robotics (2014)*, pages 1–6. IEEE, 2014.



- [3] S.-E. Tsai and S.-H. Zhuang. Optical flow sensor integrated navigation system for quadrotor in GPS-denied environment. In *2016 International Conference on Robotics and Automation Engineering (ICRAE)*, pages 87–91. IEEE, 2016.
- [4] G. Balamurugan, J. Valarmathi, and V. Naidu. Survey on uav navigation in gps denied environments. In *2016 International conference on signal processing, communication, power and embedded system (SCOPE5)*, pages 198–204. IEEE, 2016.
- [5] J. Kim, S. Sukkarieh, et al. 6dof slam aided GNSS/INS navigation in GNSS denied and unknown environments. *Positioning*, 1(09), 2005.
- [6] S. Urzua, R. Munguía, and A. Grau. Vision-based slam system for MAVs in GPS-denied environments. *International Journal of Micro Air Vehicles*, 9(4):283–296, 2017.
- [7] S. Khattak, F. Mascarich, T. Dang, C. Papachristos, and K. Alexis. Robust thermal-inertial localization for aerial robots: A case for direct methods. In *2019 International Conference on Unmanned Aircraft Systems (ICUAS)*, pages 1061–1068. IEEE, 2019.
- [8] I. Leontaritis and S. A. Billings. Input-output parametric models for non-linear systems part i: deterministic non-linear systems. *International journal of control*, 41(2):303–328, 1985.
- [9] P. Sastry, G. Santharam, and K. Unnikrishnan. Memory neuron networks for identification and control of dynamical systems. *IEEE transactions on neural networks*, 5(2):306–319, 1994.
- [10] N. Rao and S. Sundaram. Spatio-temporal look-ahead trajectory prediction using memory neural network. In *2021 International Joint Conference on Neural Networks (IJCNN)*, pages 1–8, 2021. doi:10.1109/IJCNN52387.2021.9534209.
- [11] G. Shi, X. Shi, M. O’Connell, R. Yu, K. Azizzadenesheli, A. Anandkumar, Y. Yue, and S.-J. Chung. Neural lander: Stable drone landing control using learned dynamics. In *2019 International Conference on Robotics and Automation (ICRA)*, pages 9784–9790. IEEE, 2019.
- [12] H. Vermeille. Direct transformation from geocentric coordinates to geodetic coordinates. *Journal of Geodesy*, 76(8):451–454, 2002.
- [13] P. Riseborough and Team. PX4 Estimation and Control Library. <https://github.com/PX4/PX4-ECL>, 2016.
- [14] T. Qin, P. Li, and S. Shen. Vins-mono: A robust and versatile monocular visual-inertial state estimator. *IEEE Transactions on Robotics*, 34(4):1004–1020, 2018. doi:10.1109/TRO.2018.2853729.
- [15] G. Loianno, M. Watterson, and V. Kumar. Visual inertial odometry for quadrotors on se (3). In *2016 IEEE International Conference on Robotics and Automation (ICRA)*, pages 1544–1551. IEEE, 2016.
- [16] H. Vermeille. An analytical method to transform geocentric into geodetic coordinates. *Journal of Geodesy*, 85(2):105–117, 2011.
- [17] Geodetic System. Geodetic system — the GIS encyclopedia, 2017. URL [http://wiki.gis.com/wiki/index.php/Geodetic\\_system](http://wiki.gis.com/wiki/index.php/Geodetic_system) [Online; modified 13-February-2017].
- [18] C. Karney. Geographiclib. online at <http://geographiclib.sourceforge.net>, 2015.
- [19] M. K. Al-Sharman, Y. Zweiri, M. A. K. Jaradat, R. Al-Husari, D. Gan, and L. D. Seneviratne. Deep-learning-based neural network training for state estimation enhancement: Application to attitude estimation. *IEEE Transactions on Instrumentation and Measurement*, 69(1):24–34, 2019.
- [20] A. Assad, W. Khalaf, and I. Chouaib. Radial basis function kalman filter for attitude estimation in GPS-denied environment. *IET Radar, Sonar & Navigation*, 14(5):736–746, 2020.

- [21] K. Zhu, X. Guo, C. Jiang, Y. Xue, Y. Li, L. Han, and Y. Chen. MIMU/odometer fusion with state constraints for vehicle positioning during beidou signal outage: Testing and results. *Sensors*, 20(8):2302, 2020.
- [22] C. Lindstrom, R. Christensen, and J. Gunther. An investigation of GPS-denied navigation using airborne radar telemetry. In *2020 IEEE/ION Position, Location and Navigation Symposium (PLANS)*, pages 168–176, 2020.
- [23] S. Zahran, A. Moussa, and N. El-Sheimy. Enhanced drone navigation in GNSS denied environment using VDM and hall effect sensor. *ISPRS International Journal of Geo-Information*, 8(4):169, 2019.
- [24] C. Forster, D. Sabatta, R. Siegwart, and D. Scaramuzza. RFID-based hybrid metric-topological slam for GPS-denied environments. In *2013 IEEE International Conference on Robotics and Automation*, pages 5228–5234. IEEE, 2013.
- [25] D. Scaramuzza, M. C. Achtelik, L. Doitsidis, F. Friedrich, E. Kosmatopoulos, A. Martinelli, M. W. Achtelik, M. Chli, S. Chatzichristofis, L. Kneip, et al. Vision-controlled micro flying robots: from system design to autonomous navigation and mapping in GPS-denied environments. *IEEE Robotics & Automation Magazine*, 21(3):26–40, 2014.
- [26] A. L. Majdik, D. Verda, Y. Albers-Schoenberg, and D. Scaramuzza. Air-ground matching: Appearance-based GPS-denied urban localization of micro aerial vehicles. *Journal of Field Robotics*, 32(7):1015–1039, 2015.